MATERIALS SCIENCE

Ultrathin rubbery bio-optoelectronic stimulators for untethered cardiac stimulation

Zhoulyu Rao[1,2], Faheem Ershad[3,4,5], Ying-Shi Guan[6], Fernanda C. Paccola Mesquita[7], Ernesto Curty da Costa[7], Marco A. Morales-Garza[8], Angel Moctezuma-Ramirez[8], Bin Kan[9], Yuntao Lu[2], Shubham Patel[1,2], Hyunseok Shim[2,10], Kuan Cheng[11], Wenjie Wu[12], Tahir Haideri[5], Xiaojun Lance Lian[5], Alamgir Karim[12], Jian Yang[13], Abdelmotagaly Elgalad[8], Camila Hochman-Mendez[7], Cunjiang Yu[1,2,3,4,5,14,15]*

Untethered electrical stimulation or pacing of the heart is of critical importance in addressing the pressing needs of cardiovascular diseases in both clinical therapies and fundamental studies. Among various stimulation methods, light illumination–induced electrical stimulation via photoelectric effect without any genetic modifications to beating cells/tissues or whole heart has profound benefits. However, a critical bottleneck lies in the lack of a suitable material with tissue-like mechanical softness and deformability and sufficient optoelectronic performances toward effective stimulation. Here, we introduce an ultrathin (<500 nm), stretchy, and self-adhesive rubbery bio-optoelectronic stimulator (RBOES) in a bilayer construct of a rubbery semiconducting nanofilm and a transparent, stretchable gold nanomesh conductor. The RBOES could maintain its optoelectronic performance when it was stretched by 20%. The RBOES was validated to effectively accelerate the beating of the human induced pluripotent stem cell–derived cardiomyocytes. Furthermore, acceleration of ex vivo perfused rat hearts by optoelectronic stimulation with the self-adhered RBOES was achieved with repetitive pulsed light illumination.

INTRODUCTION

Soft, deformable electronic materials or devices that could be seamlessly integrated with the heart, or a variety of electrically excitable and mechanically dynamic tissues or organs, while capable of effectively modulating biological functions in a nongenetic fashion and untethered manner are of critical importance to many fields ranging from fundamental biological studies (*1*, *2*) to medical device development (*3*) to clinical therapies (*4*, *5*). Existing methods to provide untethered electrical stimuli commonly feature the integration of implanted stimulating electrodes with untethered power modules (*6*–*8*). However, these devices are typically rigid, bulky, and complex in system architecture; thus, it is challenging to seamlessly integrate them with soft, deformable, and dynamic organs and tissues (*7*), which unavoidably causes device failure or tissue damage (*9*). For instance, conventional implantable batteries are rigid; many are bulky in size to ensure sufficient energy capacity (*10*). Recent development of wireless power transfer technologies—such as far-field radiofrequency power transfer, magnetic resonant coupling, and ultrasonic power transfer—holds promise in implantable bioelectronics, but these approaches also involve the constraints in size, shape, and/or material incompatibility of the in-body receivers (*7*). Mechano-electrical transduction that converts body or organ motions into electrical energy via triboelectric effects usually suffers from low output power and uncontrollability of the electrical stimulation signals (*11*).

On the other hand, electrical stimulation through light, e.g., via photoelectric effect, offers critical benefits including inherent untethered stimulation, readily available and versatile light sources, and no need of genetic modification (*12*, *13*). Although a few recent studies showed that conventional semiconductor materials and devices are able to stimulate cells and tissues (*12*, *14*, *15*), a critical bottleneck lies in the lack of a suitable material with tissue-like mechanical softness and deformability while offering optoelectronic performances to allow effective cardiac stimulation. Specifically, concurrent deformation [i.e., ~20% strain (*16*–*18*)] of a stimulating device with a beating heart during the stimulation while not constraining its beating is of paramount importance. However, materials and devices with these collective properties have never been developed.

Here, we report an ultrathin (thickness < 500 nm), soft, stretchy, and self-adhesive rubbery bio-optoelectronic stimulator (RBOES) for untethered optoelectronic cardiac stimulation. Specifically, the RBOES was formed in a bilayer stack of the rubbery semiconducting nanofilm based on a planar phase-separated composite of a semiconductor and an elastomer and an optically transparent and stretchable gold (Au) nanomesh conductor (Fig. 1A). The RBOES can conform to and form strong adhesion with an epicardial surface and concurrently deform with a heart while producing a photovoltage as high as 120 mV under light illumination (2.8 mW/mm^2). The RBOES could maintain its optoelectronic performance even when it was stretched by 20%. The RBOES was validated to effectively accelerate the beating

[1]Materials Research Laboratory, University of Illinois, Urbana-Champaign, Urbana, IL 61801, USA. [2]Department of Engineering Science and Mechanics, Pennsylvania State University, University Park, PA 16802, USA. [3]Department of Electrical and Computer Engineering, University of Illinois, Urbana-Champaign, Urbana, IL 61801, USA. [4]Beckman Institute for Advanced Science and Technology, University of Illinois, Urbana-Champaign, Urbana, IL 61801, USA. [5]Department of Biomedical Engineering, Pennsylvania State University, University Park, PA 16802, USA. [6]Institute of Advanced Materials, School of Chemistry and Chemical Engineering, Southeast University, Nanjing, Jiangsu 211189, China. [7]Regenerative Medicine Research Lab, Texas Heart Institute, Houston, TX 77030, USA. [8]Center for Preclinical Surgical & Interventional Research, Section of Transplantation, Texas Heart Institute, Houston, TX 77030, USA. [9]School of Materials Science and Engineering, Nankai University, Tianjin 300350, China. [10]Department of Electronics Engineering, Pusan National University, Busan 46241, Republic of Korea. [11]Materials Science and Engineering Program, University of Houston, Houston, TX 77024, USA. [12]Department of Chemical and Biomolecular Engineering, University of Houston, Houston, TX 77024, USA. [13]Department of Materials Science and Engineering, Research Center for Industries of the Future, Westlake University, Hangzhou, Zhejiang 310030, China. [14]Department of Materials Science and Engineering, Materials Research Institute, Pennsylvania State University, University Park, PA 16802, USA. [15]Department of Mechanical Science and Engineering, Materials Science and Engineering, Bioengineering, Nick Holonyak Micro and Nanotechnology Laboratory, University of Illinois, Urbana-Champaign, Urbana, IL 61801, USA.
*Corresponding author. Email: cunjiang@illinois.edu

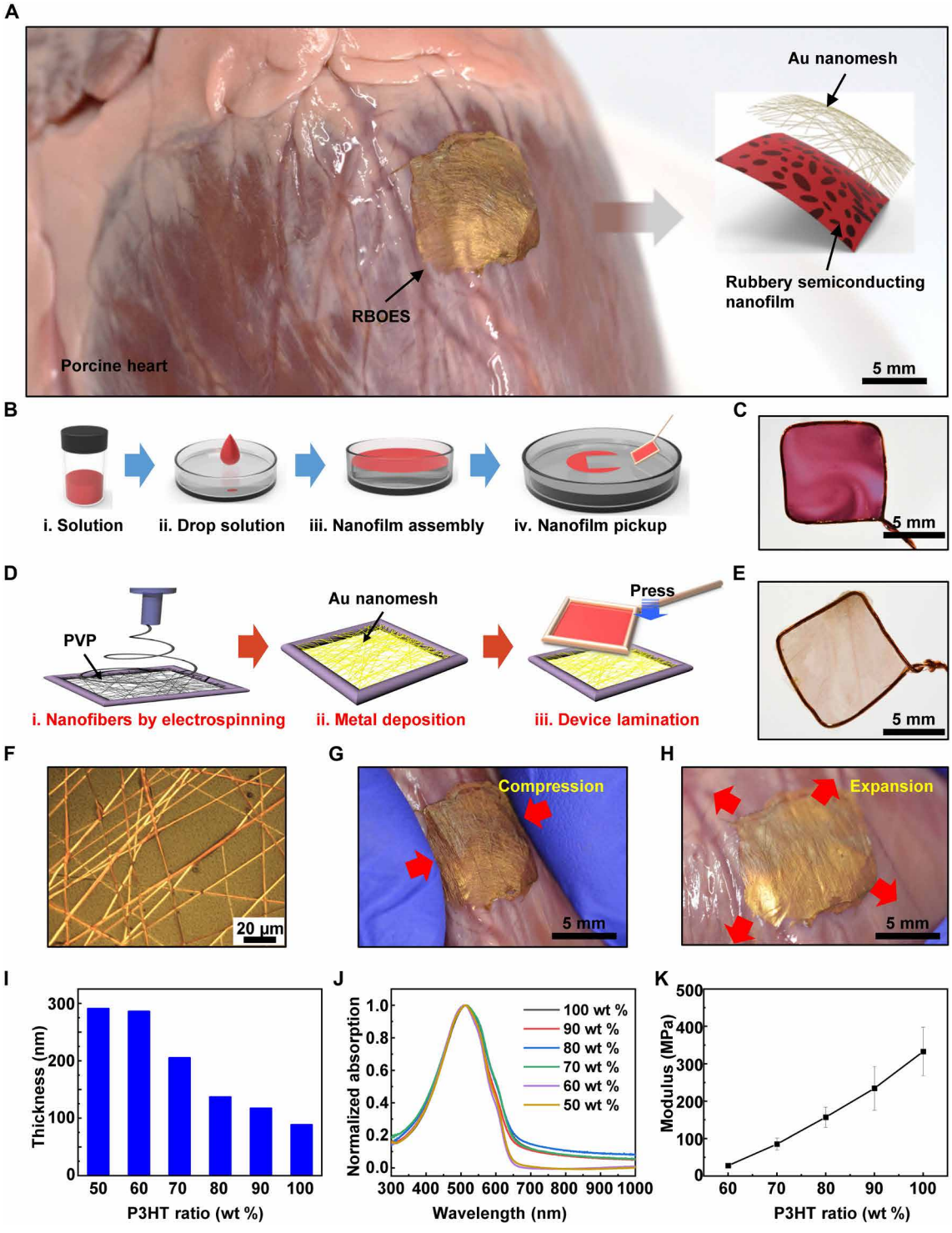

Fig. 1. The RBOES. (**A**) Optical image of the RBOES on a porcine heart surface. The RBOES conforms to the texture of the heart surface. The right inset shows the structure of the RBOES including the rubbery semiconducting nanofilm and a transparent and stretchable Au nanomesh conductor. (**B**) Schematic fabrication flow of the rubbery semiconducting nanofilm. (**C**) The as-fabricated nanofilm on a metallic frame. (**D**) Schematic fabrication flow of the RBOES by laminating the rubbery semiconducting nanofilm on the Au nanomesh to form a bilayer stack. (**E**) RBOES assembled on a metallic frame. (**F**) Microscopic image of the RBOES. (**G** and **H**) RBOES was maintained on the cadaver porcine heart surface under compression (G) and expansion (H) conditions, respectively. (**I**) Thicknesses of the nanofilms with different compositions. (**J**) Normalized absorption of the nanofilms with different compositions. (**K**) Tensile moduli of the nanofilms with different compositions, the calculated moduli are fitted by the linear region of the stress-strain curves. Error bars represent the SEM from five samples.

of the human induced pluripotent stem cell–derived cardiomyocytes (hiPSC-CMs). Furthermore, optoelectronic stimulation was accomplished on perfused rat hearts based on the self-adhered RBOES with repetitive pulsed light illumination.

RESULTS

RBOES fabrication and characterization

In the device configuration, the rubbery semiconducting nanofilm can form a photoelectrochemical interface with biological fluids, and the Au conductor can form an ohmic contact with the rubbery semiconducting nanofilm and ensure efficient hole collection and optoelectronic characteristics of the nanofilm-electrolyte interface (*19*, *20*). We selected the organic semiconducting film in a rubbery format because it provides not only the optoelectronic function but also the mechanical softness, inherited from the two components. The similarity of the material softness to that of the native tissue is preferable for paced CM development (*21*). To provide stimulation to the target tissue, the rubbery semiconducting nanofilm side should contact the biological fluids and tissues during optical stimulation, while the light is illuminated from the electrode side. Therefore, the conductor must be transparent and stretchable to allow the light to penetrate to the semiconducting nanofilm. Specifically, the Au nanomesh conductor was chosen to build the RBOES over other transparent conductors such as semi-transparent Au films, poly(3,4-ethylenedioxythiophene)-poly(styrenesulfonate), and indium tin oxide, owing to its extraordinary softness and relatively larger stretchability (*22*).

The rubbery semiconducting nanofilm, composed of the poly(3-hexylthiophene-2,5-diyl) (P3HT) semiconductor and polystyrene-block-poly(ethylene-ran-butylene)-block-polystyrene (SEBS) elastomer, was prepared using the air/water interfacial assembly method (Fig. 1B and Materials and Methods), which is facile and scalably manufacturable. Briefly, the P3HT/SEBS toluene solution was gently dropped onto the water surface, which spread out rapidly and consequently self-assembled into a well-ordered and thin nanofilm at the air-water interface due to the Marangoni effect. The free-standing rubbery semiconducting nanofilm was held by a metallic frame for further handling (Fig. 1C). The resulting nanofilm shows planar binary phases (fig. S1). The continuous region is identified as the P3HT-rich domain, and the isolated region is identified as the SEBS-rich domain (fig. S2). The Au nanomesh was prepared by coating a thin layer of Au (100 nm) on top of the electrospun polymer web (Fig. 1D and fig. S3, A and B). The sheet resistance of the Au nanomesh slightly increased under tensile strains from 0 to 30% (fig. S3C). Last, the RBOES was formed by laminating the two components to form a stack (Fig. 1E and fig. S4). Figure 1F shows a microscopic image of the prepared RBOES. The device can be conformably placed on the epicardial surface of a living rat heart (movie S1) and cadaver porcine heart under deformation (Fig. 1, G and H).

The thickness of the nanofilms with 100, 90, 80, 70, 60, and 50 weight % (wt %) of P3HT are 87.8, 116.8, 136.5, 204.6, 285.6, and 290.3 nm, respectively (Fig. 1I). The ultrathin nanofilm with 60 wt % P3HT can hold a water droplet, which is 90,000 times heavier than its own weight (fig. S5). The Au nanomesh has a total thickness of <200 nm (fig. S6). Thus, the resulted RBOES from the stack of the nanofilm and Au nanomesh is less than 500 nm after assembling the two components. The Au nanomesh is highly transparent (fig. S7), and all the rubbery semiconducting nanofilms have similar maximum optical absorption peaks (Fig. 1J). As the core material of the RBOES and the interface to the biological tissues, the rubbery semiconducting nanofilm dominates the mechanical property and adhesion of the RBOES. The rubbery semiconducting nanofilms with a relatively lower wt % of P3HT can tolerate 50% mechanical strain without generating any cracks (fig. S8). In contrast, cracks were present in the nanofilms with a higher wt % of P3HT when stretched by 50%. The strain-stress curves of the rubbery semiconducting nanofilms with different compositions were measured (fig. S9, A and B, and Materials and Methods). The calculated moduli of the nanofilms with 100, 90, 80, 70, and 60 wt % of P3HT are 333, 234, 157, 85, and 28 MPa, respectively (Fig. 1K). Rubbery semiconducting nanofilms with a low wt % of P3HT show excellent rubber-like mechanical softness and low moduli, which are close to those of the porcine heart tissue. The aforementioned ultrathin thickness and rubber-like modulus endow the rubbery semiconducting nanofilms with a high degree of self-adhesiveness due to the surface tension of the liquid (*23*). Separation forces of 10 to 13 mN from a porcine heart surface were observed for the rubbery semiconducting nanofilms (fig. S10, A to C), which are more than 100,000 times higher than the nanofilms' weight. The ultrathin, soft, stretchy, and self-adhesive rubbery semiconducting nanofilm is advantageous and a favorable candidate for biological interfaces, which allows for conformability and self-adhesiveness to arbitrarily shaped and rough surfaces (*24*–*27*), also evidenced by its conformability on wrinkled human skin (fig. S11).

We next evaluated the optoelectronic performances of the rubbery semiconducting nanofilms with different compositions on the Au film. At the nanofilm-electrolyte interface, the electrochemical potential (identified as the Fermi level in electrolyte) and Fermi level reach equilibrium. Equilibration of this interface thus necessitates the flow of charge from one phase to the other due to the surface polarization by absorbed water molecules on the surface of the nanofilm layer, and the band bending of the highest occupied and the lowest unoccupied molecular orbitals appears within the semiconductor phase (Fig. 2A) (*28*). The total potential difference across this interface is related to the carrier concentration in P3HT and redox potential of the electrolyte. Upon light illumination, electron-hole pairs are generated at the interface, where electrons move toward the electrolyte and holes move to the nanofilm/Au, which is evidenced by a negative current at the electrolyte side (Fig. 2B and Materials and Methods). The photovoltages of different rubbery semiconducting nanofilm–based devices were characterized. We tested the photovoltages with a shunt resistor of 47 kohm (fig. S12A) (*29*). The device based on the 90 wt % P3HT shows a maximum photovoltage of 190 mV (Fig. 2C). Besides, the photovoltages decrease as the wt % of P3HT decreases. The degradation in the photovoltages may result from the change of the charge mobility and active layer light absorption (*30*). We then tested the device performances at different pulse durations (Fig. 2D), light intensities (Fig. 2E), and pulse frequencies (Fig. 2F). The photovoltages reached the peak value at 20-ms pulse and decreased at a longer pulse. As the irradiance increased, the photovoltages increased. At a pulse frequency higher than 1 Hz, the photovoltages were affected by repetitive illumination, and their magnitude decreased as the frequencies increased (*31*). The Au film-electrolyte interface under the same condition provided no optoelectronic effect (fig. S12B). Moreover, no decay in the generated photovoltages was observed with a continuous 300-pulse illumination (Fig. 2G).

The optoelectronic property of the RBOES was characterized using similar procedures to those in the previous section. Liquid metal

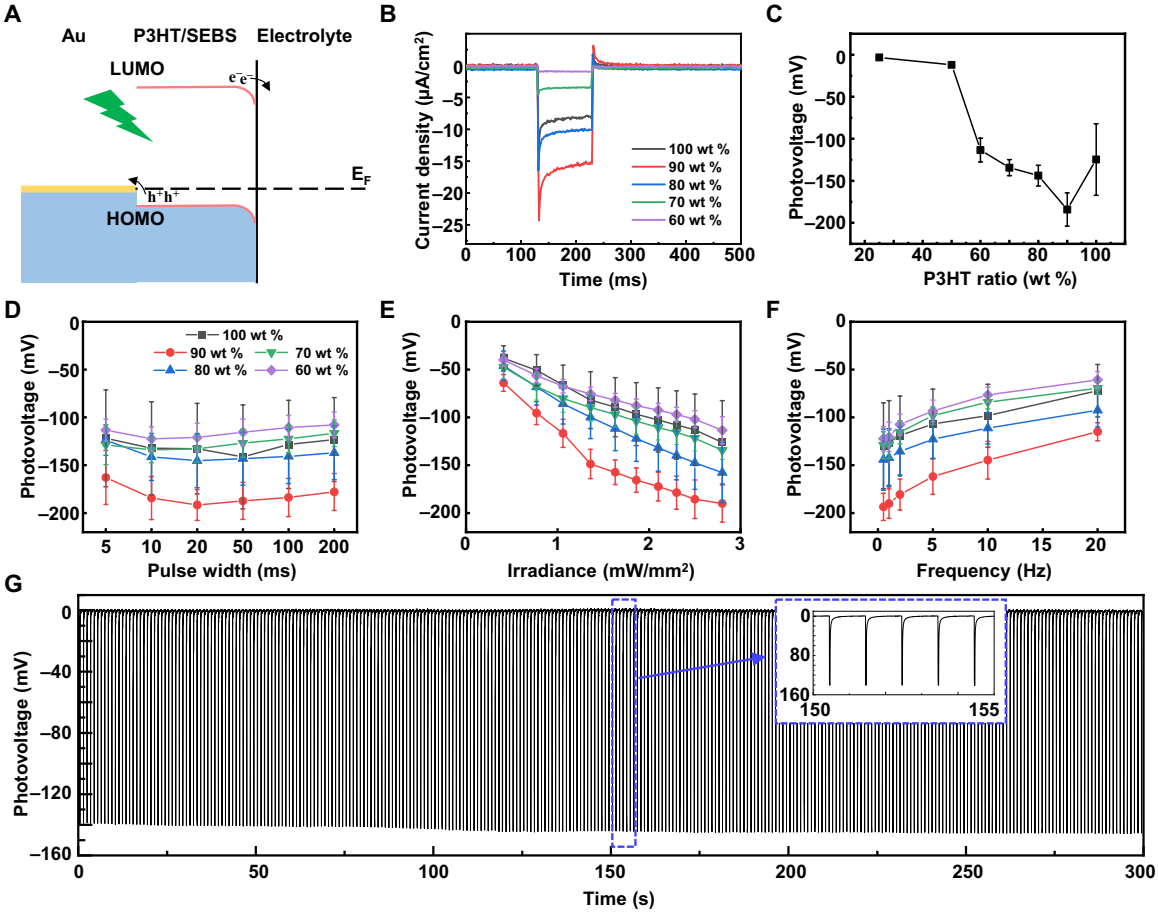

Fig. 2. Photoelectric assessment of rubbery semiconducting nanofilms. (**A**) Band diagram of the polarized rubbery semiconducting nanofilm-electrolyte interface. HOMO and LUMO: highest occupied and the lowest unoccupied molecular orbitals, respectively. (**B**) Current densities obtained from interfaces with different compositions of nanofilms under pulsed light illumination (1 Hz, 100 ms, and 2.8 mW/mm^2). (**C**) Photovoltages obtained from different rubbery semiconducting nanofilm based interfaces (530 nm, 2.8 mW/mm^2). Error bars represent the SEM from five devices. (**D** to **F**) Photovoltages from different wt % of P3HT-based interfaces measured upon illumination with pulse durations (5, 10, 20, 50, 100, and 200 ms), light intensities (up to 2.8 mW/mm^2), and frequencies (1 to 20 Hz), respectively. Error bars represent the SEM from five devices. (**G**) Photovoltage of the nanofilm-electrolyte interface based on 100 wt % P3HT upon illumination for 300 s (1 Hz, 20 ms, and 2.8 mW/mm^2).

was used to ensure proper contact with the Au nanomesh (Fig. 3A). Because of the transparency of the Au nanomesh (*32*, *33*), the RBOES can receive the light shone from the electrode side (fig. S13), which allows the nanofilm side to contact the biological tissues. Similar to the abovementioned results, photovoltages elicited from the 90 wt % P3HT RBOES reached a peak of 120 mV. The photovoltages decreased as the wt % of P3HT decreased (Fig. 3B). However, the amplitudes of the photovoltages from RBOESs are smaller than that of the corresponding Au/nanofilm-electrolyte interfaces, which is due to the smaller effective area of Au in the nanomesh as compared to the Au film. The performances of the RBOES at different pulse durations (Fig. 3C), light intensities (Fig. 3D), and pulse frequencies (Fig. 3E) showed similar trends to that of the rubbery semiconducting nanofilms on an Au film. The morphology of the nanofilm shows no difference after 10-min light illumination (fig. S14, A to C).

The optoelectronic characteristics of the RBOES under different levels of mechanical strain were also studied. In the rubbery semiconducting nanofilms with 100, 90, and 80 wt % of P3HT, micron-sized cracks were present after 20% stretching (Fig. 3F). In contrast, no obvious crack was observed in rubbery semiconducting nanofilms with 70 wt % P3HT. Considering the mechanical stretchability, modulus, and optoelectronic performance, the RBOES constructed with 70 wt % P3HT was chosen for further investigation and biological modulation. The photovoltages of the RBOES with 70 wt % P3HT were tested under long-term pulsed light illumination (fig. S15, A to C). The RBOES with 70 wt % P3HT was stretchable up to 20% and no crack was observed in the nanofilm and Au nanomesh (Fig. 3G). The RBOES retained optoelectronic functions even under 20% applied mechanical strain (Fig. 3H). When the RBOES was stretched by 10%, the photovoltages decreased to 87% of the value without any strain. The photovoltage decreased to 68% when placed under 20% strain. The photovoltage maintained 78% of the original when the stretching was released. The photovoltage of the RBOES with 70 wt % P3HT shows its high stability during cyclic stretching (stretched at 20% for 1000 cycles; fig. S15D).

In vitro stimulation of hiPSC-CMs

Human iPSC-CMs with high expression of cardiac troponin T (cTNT) were used to validate the operation of the RBOES in vitro

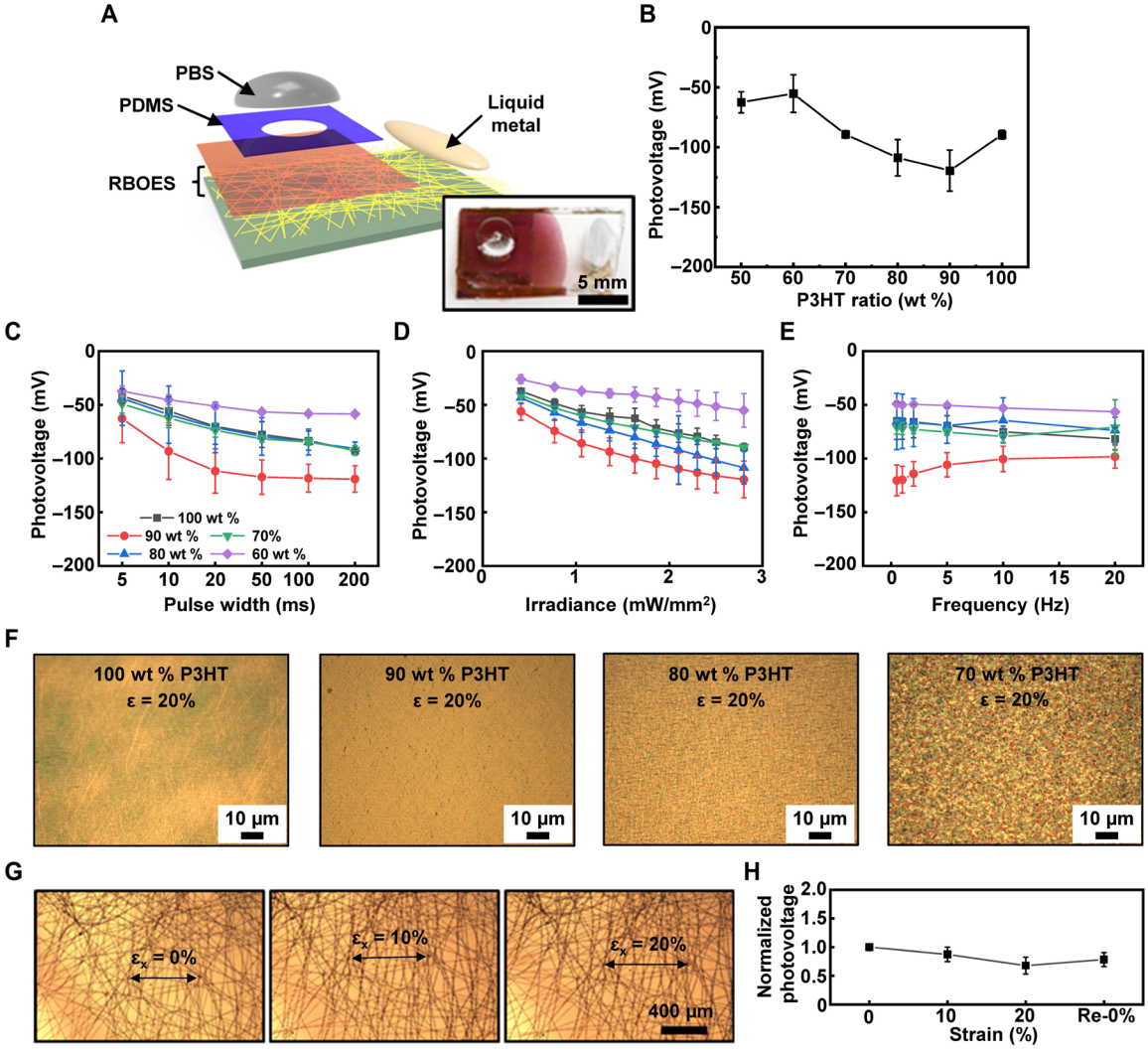

Fig. 3. Characterization of the RBOES. (**A**) Schematic illustration of the measurement setup. The two electrodes are connected to the phosphate-buffered saline (PBS) and liquid metal. The inset shows the microscopic image of the RBOES. Scale bar, 5 mm. (**B**) Photovoltages obtained from RBOES based on different compositions of nanofilms under a pulsed light (1 Hz, 100 ms, and 2.8 mW/mm^2). Error bars represent the SEM from five devices. (**C** to **E**) Photovoltages from different wt % of P3HT obtained from RBOES measured upon illumination with different pulse durations (5, 10, 20, 50, 100, and 200 ms), light intensities (up to 2.8 mW/mm^2), and frequencies (1 to 20 Hz), respectively. Error bars represent the SEM from five devices. (**F**) Optical images of the rubbery semiconducting nanofilms with different wt % of P3HT under 20% strain. (**G**) Microscopic images of the RBOES with 70 wt % P3HT under different tensile strains from 0 to 20%. (**H**) Photovoltages of the RBOES under tensile strain. Error bars represent the SEM from five devices. PDMS, polydimethylsiloxane.

(fig. S16A). The viability of the cells was first evaluated after 5 days of culture with the RBOES. Figure 4A shows the stained nuclei [using 4′,6-diamidino-2-phenylindole (DAPI)] of the CMs on the RBOES. A LIVE/DEAD viability assay (Fig. 4B) and the expression of cTNT (fig. S16B) were used to quantify the cell survival in the presence of the RBOES before stimulation. No substantial differences were found in both cell viability [93.76 and 93.98% for the control (red) and RBOES (blue) group, respectively, $n = 4$; Fig. 4B] and in the expression of cTNT [without RBOES, 79.43 ± 3.66% (red) and with RBOES, 80.5 ± 6.35% (blue) plated in RBOES], indicating that the RBOES does not cause cytotoxicity in the CMs. Afterward, the RBOES with 70 wt % P3HT was investigated with optoelectronic stimulation capabilities on a monolayer of CMs (Fig. 4C and Materials and Methods). The whole measurement system was placed in an incubator to maintain the typical culture conditions. The RBOES without CMs was first placed on a multielectrode array (MEA) plate (fig. S17, A to C). Upon illumination with a repetitive pulse of 1 Hz on the RBOES, only the channels covered by the RBOES generated potential signals (fig. S17, D and E), and the potential signal of a representative channel was consistent with the optical stimuli (Fig. 4D). The hiPSC-CMs were then cocultured with the RBOES on an MEA plate (Fig. 4E). The responses from the RBOES and electrocardiography (ECG) from CMs were both observed during the optoelectronic stimulation (Fig. 4F). Briefly, each stimulation period used the following protocol (Fig. 4G): 1 min of recording spontaneous ECG before stimulation, followed by 10 min of optoelectronic stimulation with simultaneous recording, and then 1 min of recording spontaneous ECG without stimulation. In

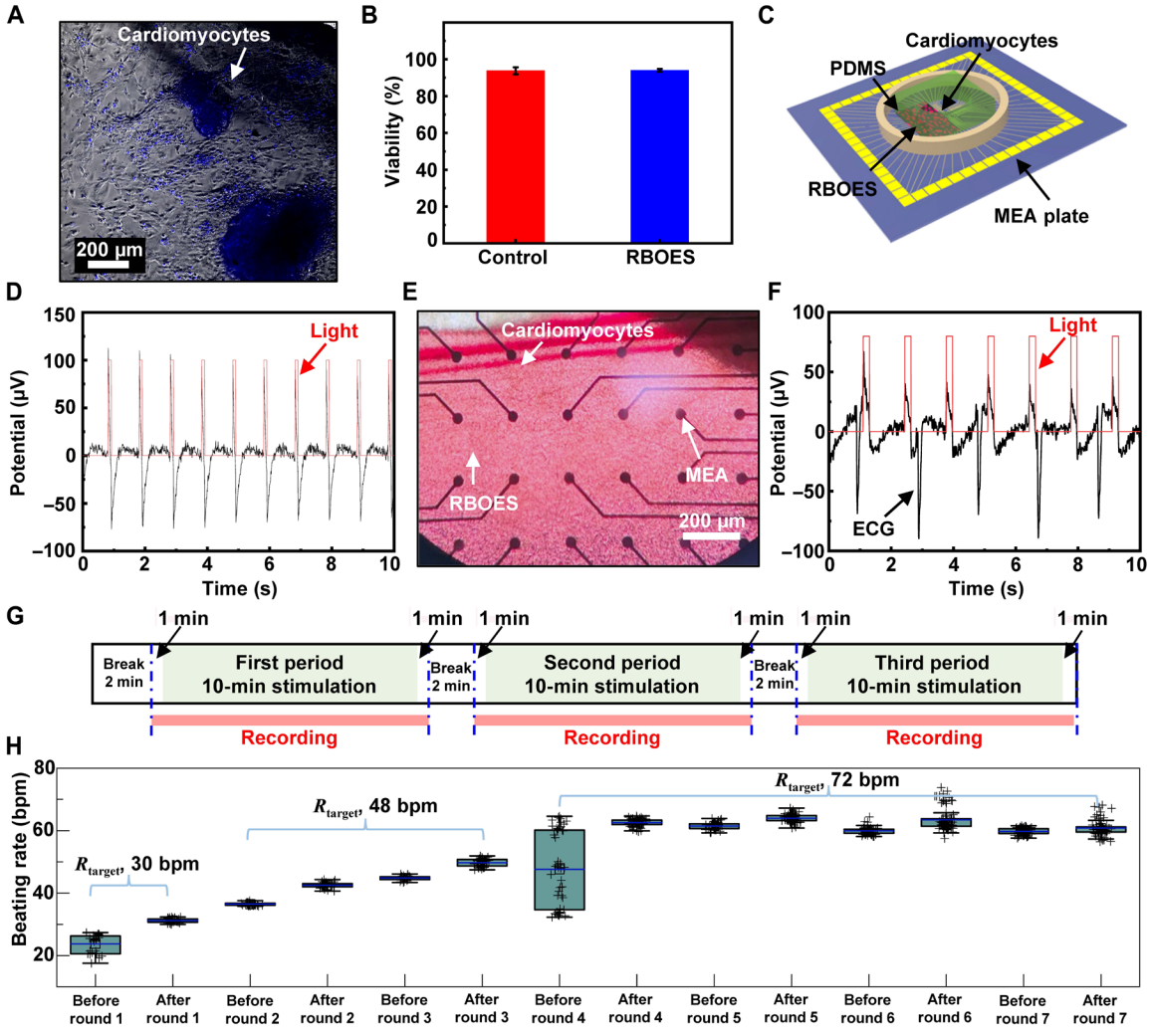

Fig. 4. Optoelectronic stimulation of the CMs by the RBOES. (**A**) 4′,6-diamidino-2-phenylindole staining with overlay of CMs cultured on the RBOES. Blue colored dots indicate viable cells. (**B**) Statistical analysis of cell viability on control (red) and RBOES-coated (blue) substrates ($n = 4$). (**C**) Schematic illustration of the optical stimulation of the CMs by the RBOES and recording by the MEA system. (**D**) Potential signal of the representative channel covered by the RBOES without cells under the optical stimuli. (**E**) Image of cultured CMs on the RBOES in the MEA plate. (**F**) Responses from the RBOES and representative ECG signal of CMs during the optical stimulation before the target beating rate of CMs was achieved. The red line represents the light pulse. (**G**) Illustration of the optoelectronic stimulation protocol with 1 min of prestimulation recording, followed by 10-min optoelectronic stimulation with simultaneous recording, 1-min post-stimulation recording, and 2-min break period between two stimulation periods. (**H**) Beating rate of CMs of a representative group before and after optoelectronic stimulation with a series of targeted beating rates (total of seven rounds with R_{target}, 30, 48, and 72 bpm).

between each stimulation period, i.e., gaps between the panels in Fig. 4H, break periods of 2 min were added to minimize cytotoxic effects (*12*). Further details are provided in Materials and Methods. A representative group of CMs [the initial beating rate was 20 to 30 beats per minute (bpm)] was stimulated under consecutive stimulation periods with a series of targeted beating rates [total of 7 rounds with 30-, 48-, and 72-bpm target rate (R_{target})]. The average beating rates before and after stimulation in each round are presented in Fig. 4H. In Fig. 4H, each data point represents the beating rate of CMs near one channel of the MEA plate. Initially, the beating rate was not synchronous before optical stimulation, which is a typical characteristic of healthy hiPSC-CMs (*34*). Upon stimulation, the CM beating rate becomes synchronous and gradually accelerated toward the targeted beating rate after stimulation (the real time beating rate in each round is shown in fig. S18). To achieve a higher targeted beating rate within the physiological range, more stimulation periods were required (*12*). The CMs demanded 1, 2, and 4 stimulation periods to achieve 30, 48, and 72 bpm, respectively.

As expected, the MEA electrodes recorded the propagation of the ECG signal of CMs without stimulation and with optoelectronic stimulation. The conduction time delays of ECG signals before and after optoelectronic stimulation was observed (fig. S19 in the horizontal direction and fig. S20 in the diagonal direction). The activation maps from all the MEA electrodes during optoelectronic stimulation with different target frequencies demonstrate clear propagation of activation time decrease from the top left to the bottom right side of the MEA (fig. S21). It is noted that the beating rate under optoelectronic stimulation at a frequency of 1.2 Hz (72 bpm) was maintained

for approximately 100 s in seventh round stimulation and then stabilized at ~60 bpm for the remainder of the 1.2-Hz stimulation. Two types of signals were observed in the first three stimulation periods at 1.2 Hz, and the slower ECG signals were considered as the intrinsic rate of CMs (details of ECG signal in the first period at 1.2-Hz stimulation are shown in fig. S22). Therefore, the first three stimulation periods are the transition stages to the target beating activity, which are evidenced by the gradual decrease of the intrinsic rate of CMs in the first three stimulation periods and the disappearance of the intrinsic rate of CMs in the fourth stimulation period. After removing the optoelectronic stimulation, the beating rate either suddenly dropped to the prestimulation beating rate (end of the fourth stimulation period for 1.2-Hz stimulation) or continued at the targeted rate (for 0.5 and 0.8-Hz stimulation). In addition, CMs cultured without the RBOES did not respond to the light stimuli with a targeted frequency, presenting neither synchronized beating (fig. S23A) nor an accelerated beating rate (fig. S23B). Although further thorough study is required to uncover the detailed mechanism of the optoelectronic stimulation, we hypothesize here that the optoelectronic stimulation is similar to an electrical stimulation with a voltage below the threshold required for triggering the myocardial excitation, i.e., subthreshold stimulation (*35*). When illuminated, charges generated by the RBOES push the unstable membrane potential of pacemaker cells closer to the threshold voltage. This process increases the slope of phase four, similar to sympathetic effects of the autonomic nervous system (*36*), and decreases the time required to reach the threshold voltage, which increases the pacemaker depolarization rate. Repetitive pulses over time "train" the cells to begin beating closer to the physiologically acceptable target frequency. This hypothesis explains why cells gradually match the rate of stimulation (*12*, *37*). These results demonstrate effective modulation and acceleration capabilities of the RBOES for the cultured CMs.

Ex vivo stimulation of perfused rat hearts

Because of the different environments between an electrolyte solution and tissues from organs, we next examined the photovoltage of the RBOES on a porcine cadaver heart tissue and an intercostal nerve. The porcine cadaver heart tissue resided in a similar physiological environment to that of a perfused rat heart (Fig. 5A). A corresponding pulse potential was recorded from the cadaver heart tissue under pulsed light illumination (Fig. 5B). Furthermore, this generated potential could propagate through the intercostal nerve serving as a conduction path to transport voltage elicitation (Fig. 5C). Upon application of optoelectronic stimulation at the middle of the nerve, the recorded signals indicated that the nerve conducted the stimulation to each end (Fig. 5D and fig. S24, A and B). As a control, when the light was applied to the nerve without the RBOES, no response was detected (fig. S24C). These results suggest that the RBOES could effectively stimulate nerve tissues.

As a proof of concept, we further validate the RBOES on perfused rat hearts. The mechanical softness, stretchability, ultrathin, and adhesive nature of the RBOES allow concurrent deformation with a beating heart while posing negligible mechanical constraint to the heart (*17*, *24*, *38*, *39*). The RBOESs were placed to the curvy epicardial surface of adult rat hearts maintained by a customized Langendorff setup. The heart was placed in an incubator to stabilize the temperature throughout the entire experiment because it had to be exposed to allow access for the stimulating light source (Fig. 5E and fig. S25A). The RBOESs conformably adhered to the wet curvilinear epicardial surface of the rat hearts (Fig. 5F). We did not observe any slippage of the RBOES on the heart surface, owing to the conformal contact and the strong adhesion between the two. The perfused rat heart (initial beating rate of 115 bpm) was optoelectronically accelerated with a targeted frequency of 2 and 2.5 Hz for 40 min (Fig. 5G and fig. S25B). An equivalent circuit model of the optoelectronic stimulation is shown in fig. S26. Upon stimulation, the beating rate was gently accelerated and kept steady for a relatively long duration. Afterward, the beating rate experienced a quick rise and lastly matched the targeted frequency. A similar gradual increase in the beating rate was obtained using subthreshold optical stimulation (*12*). Before stimulation, the heart beating was not periodic with an approximate beating rate of 115 bpm (Fig. 5H, top left). After 10-min optical stimulation, the beating reached the same frequency as the light pulse (2 Hz, middle at the top row in Fig. 5H). A typical ECG morphology with PQRST waves was recorded (Fig. 5I). It is noted that this phenomenon was only found in a short time during the late period of stimulation. After removing the stimulation, the targeted beating rate was maintained (Fig. 5H, top right). Similar results showing that the beating rate reached 150 bpm were found when the rat heart was stimulated at a higher frequency of 2.5 Hz (bottom row in Fig. 5H). It is noted that perceived time differences between the light pulse and ECG signals vary in the stages of optoelectronic stimulation, while the cycle lengths of ECG signals become shorter and lastly reach the same interval of the light pulses. We also exposed the heart to pulsed illumination without applying the RBOES and observed no distinct increase in beating rate during 13 min of optical illumination (fig. S27). Meanwhile, the surface temperature of the perfused rat hearts was maintained at a steady value (fig. S28). These results eliminate any possible light or temperature-induced side effects on the heart beating. In summary, optical stimulation via RBOES has been demonstrated to be a comfortable and feasible method for rat heart ex vivo stimulation. By miniaturizing the light delivery system and optimizing it for wearable/implantable optoelectronic stimulation, this RBOES could eventually stimulate hearts in vivo to offer nongenetic, remote therapy without any restraints to the wearer.

DISCUSSION

In summary, we developed an ultrathin, stretchy, and self-adhesive RBOES with combined mechanical softness and optoelectronic characteristics that are ideal for untethered cardiac stimulation using light. Systematic investigation on the material composition, mechanical properties, and optoelectronic performances illustrated key features of the RBOES. We validated the RBOES to optically accelerate the beating of the CMs in an untethered manner. We also demonstrated effective modulation of the beating rate of perfused rat hearts. Optoelectronic stimulation by the RBOES in this study affects the cell/tissues at a voltage lower than the threshold voltage typically required for conventional electrical stimulation. Unlike conventional electrical stimulation, this subthreshold stimulation exerts a mild and gradual influence on cardiac cells/tissue. The gentle nature of this subthreshold stimulation renders it appropriate for prolonged stimulation application, reducing the risk of inducing cardiac damage. It is also noted that the beating heart experiments demonstrated here were performed ex vivo in an acute manner to deliver temporary stimulation to resolve arrhythmic conditions. Thus, the current way to deliver pulsed light may be a challenge in

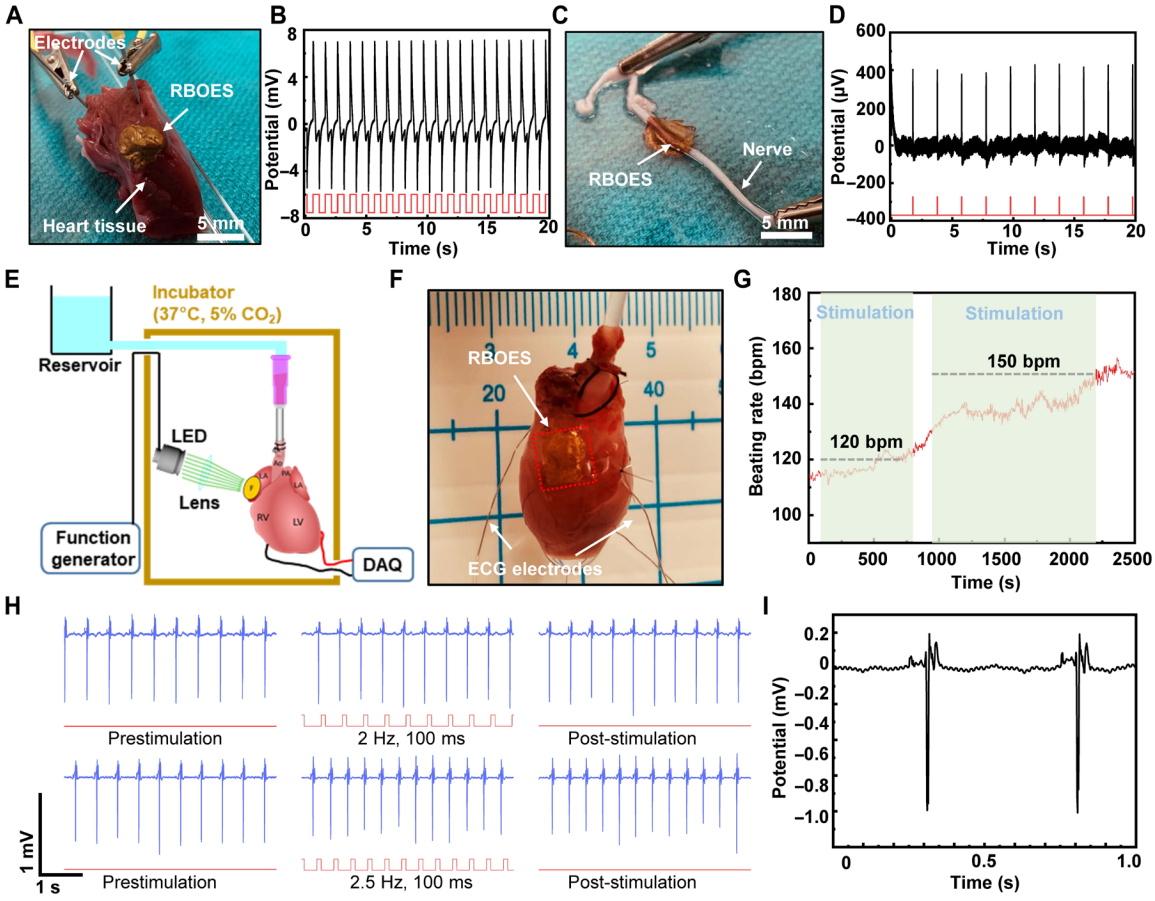

Fig. 5. Optoelectronic stimulation of perfused rat hearts. (**A** and **B**) RBOES was interfaced to the cadaver heart tissue (A) and the potential response under the light stimulation (1 Hz, 100 ms) (B). (**C** and **D**) RBOES was interfaced to an intercostal nerve (C) and the potential response under the light stimulation (0.5 Hz, 100 ms) (D). The rubbery semiconducting nanofilm side was directly placed on the tissues to form the interface. The potential signals were extracted using a pair of clamp recording electrodes. (**E**) Schematic of the measurement setup including a Langendorff system that maintained the rat hearts. An adult rat heart was placed in an incubator (37°C and 5% CO_2), and oxygenated Krebs-Henseleit buffer reservoir was perfused into the aorta of the heart. A 530-nm LED light was focused through an amplifying lens on the RBOES placed onto the exposed myocardium on the right atrium. ECG electrodes were sutured on the heart to record the signals with a data acquisition system. (**F**) Optical images of the perfused rat heart with the RBOES (marked in the dotted square) and the ECG electrodes. (**G**) Real-time beating rate of the perfused rat heart under consecutive stimulation with targeted beating rates of 120 and 150 bpm (marked in the dotted black line). (**H**) ECG signals of the perfused rat heart under optoelectronic stimulation. The top row shows the ECG signals obtained from prestimulation (0 to 5 s), during stimulation (680 to 685 s), and post-stimulation (771 to 776 s) of 2-Hz light illumination. The bottom row shows ECG signals of the perfused rat heart obtained from prestimulation (600 to 605 s), during stimulation (2240 to 2245 s), and post-stimulation (2262 to 2267 s) of 2.5-Hz light illumination. (**I**) Typical ECG with PQRST waves was observed in the signal during stimulation in (H).

the clinical setting. This could be potentially overcome by using an implantable light source with a wireless power transmission strategy (*40*, *41*). Although red or near infrared light have longer tissue penetration depths, red or near-infrared light stimulation on current version RBOES may require much higher intensity light due to relatively low absorption in the spectra. We outlook that the method to build RBOES here can be extended to build a promising stimulator based on organic semiconductors with absorption peaks in the red or near infrared spectra. In addition, RBOES with proper materials that can be biodegradable with programmable length of time period could shed light on long-term stimulation usages. Although optogenetics can be used to optically modulate biological tissues (*41*–*43*), genetic engineering is not always feasible and may cause potential functional alterations, as well as ethical and safety concerns. This work exploits an unprecedented cardiac stimulator in a rubber format developed through material engineering to form a unique rubbery semiconducting nanofilm based bio-optoelectronic interface for nongenetic biological stimulation. The RBOES is applicable to various electrically excitable tissues and organs, such as the brain, spinal cord, peripheral nerves, and skeletal muscles, which pave the way toward nongenetic, untethered stimulation for both fundamental biological studies and clinical therapy.

MATERIALS AND METHODS

Materials

Anhydrous toluene (>99%), SEBS, and polyvinylpyrrolidone (PVP; molecular weight, ~130,000) were all purchased from Sigma-Aldrich and used as received. Regioregular P3HT (rrP3HT) was purchased from Sigma-Aldrich and washed and filtered to remove the low–molecular weight rrP3HT using cyclohexane. Polydimethylsiloxane (PDMS) silicone (Sylgard 184 silicone elastomer kit) was from Dow Corning.

Preparation of rubbery semiconducting nanofilm

P3HT/SEBS composite solution was prepared by dissolving P3HT and SEBS powders with different wt % in the toluene (10 mg/ml) at 60°C and stirring overnight. To make a rubbery semiconducting nanofilm on the water surface, 20 μl of the composite solution was dropped on the water surface in a 60-mm diameter petri dish in the fume hood (nanofilm area of 28.27 cm^2 with weight of 0.2 mg, the area density is 0.007 mg/cm^2). The composite dropped on the water surface was spread spontaneously and rapidly because of the Marangoni effect. Afterward, the toluene solvent evaporated and the uniform nanofilm remained on the water surface. The nanofilm was then picked up either by a custom-built copper frame for further device fabrication or by a clean glass slide for characterization (thickness, absorption, etc.).

Preparation of Au nanomesh

The fabrication process for the Au nanomesh conductor was similar to the reports elsewhere (*24*, *44*, *45*). A PVP nanofiber template was first prepared by electrospinning. The PVP solution (10 wt %) was obtained by adding PVP powders into pure ethanol solvent and then stirring overnight at ambient temperature to form a clear solution. A custom-made electrospinning system was used to electrospin the PVP nanofibers. The PVP solution was filled in a 3-ml syringe with a 20-gauge metallic needle. The ground was connected to a square stainless-steel frame with a dimension of 2 cm by 2 cm to collect the nanofibers. The distance between the needle tip and square frame collector was fixed at 17 cm, and the applied voltage was 17 kV. The feeding rate of the PVP solution was 3 μl/min. The electrospinning time was approximately 0.5 to 1 min. Last, a 100-nm-thick Au layer was deposited on the surface of the PVP nanofibers using an electron-beam evaporator to form the conductor. The electrical conductivity of the Au nanomesh under stretching was recorded by a semiconductor analyzer (Keithley 4200-SCS, Tektronix Inc.).

Preparation of RBOES

To form a RBOES, a rubbery semiconducting nanofilm and an Au nanomesh conductor were manually assembled. The metallic frame was gently pressed down to pass through the Au nanomesh on the square frame. The Au layer on the top of the PVP fibers was directly contacted with the rubbery semiconducting nanofilms during assembling.

Atomic force microscopic characterization of rubbery semiconducting nanofilm

The rubbery semiconducting nanofilm was transferred on a silicon wafer from water for this test. The atomic force microscopic images were then acquired from Bruker's dimension icon instrument with TESPA-V2 probes at room temperature. The scanning area was 10 μm by 10 μm, and the scan rate is 1 Hz. The acquired images were analyzed with NanoScope Analysis software. The adhesion images, indentation, and modulus images were obtained at the same time. The indentation is used to measure the mechanical properties of rubbery optoelectronic nanofilm. By measuring the force required to push the diamond tip into the material compared to the depth of the indentation, the hardness of the P3HT can be determined.

Characterization of rubbery semiconducting nanofilm

The thicknesses of the rubbery semiconducting nanofilms with different weight ratios on the glass were tested by Alpha-Step IQ Surface Profiler (KLA Corporation). The absorption of the obtained rubbery semiconducting nanofilms was tested by the ultraviolet-visible (UV-vis) spectrum (Cary 5000 UV-Vis-NIR, Agilent Technologies Inc.). The stress-strain characterization was performed with a Mark-10 test system equipped with ESM 303 and a high-resolution force gauge (M5-012, Mark-10 Corp.) under continuous application of tensile strain with a speed of 0.5 mm/min and a sampling rate of 7000 points per second. During stretching, the rubbery semiconducting nanofilms were mounted on the customized PDMS clamps (fig. S9A). The engineering stress was used to calculate the tensile modulus.

Adhesion evaluation

The pulling force was recorded as a function of the travel. The adhesion evaluation of the RBOES on a wet porcine heart surface was performed using a Mark-10 test system equipped with ESM 303 stand and Series 5 force gauge (M5-012, Mark-10 Corp.). The metallic frame (diameter: 15 mm) supporting the rubbery semiconducting nanofilm was fixed onto the clamp of the force gauge. After the nanofilms were carefully attached to the surface of a porcine heart (obtained from a grocery store), the clamp was slowly lifted at constant speed of 0.5 mm/min until complete separation from the heart surface.

Current measurement

Current measurement was performed using an Autolab electrochemical station (Metrohm, USA) at room temperature and ambient pressure. The chronoamperometric measurement was performed through a two-electrode system consisting of a platinum wire as the counter electrode and a tungsten tip connected to the Au layer as the working electrode. The platinum electrode was immersed in phosphate-buffered saline (PBS) medium (pH = 7.2; Sigma-Aldrich) in a PDMS reservoir with a diameter of 5 mm at room temperature. A green light-emitting diode (LED) (M530L4-C5, Thorlabs Inc.) was shone from the top of the liquid and controlled through a function generator with a frequency of 1 Hz and a pulse width of 100 ms. The data were acquired using the NOVA software.

Photovoltage measurement

To measure the photovoltage, the rubbery semiconducting nanofilm was placed on the top of Au film or Au nanomesh on the glass. The photovoltages were recorded based on a National Instrument setup with a green LED light (emission peak at 530 nm, ~2.8 mW/mm^2, shone from the solution side). The light passed through an amplifying lens to focus on the small spot atop the nanofilm. The optical power of the LED light was measured with an optical power meter (PM100A equipped with S302C, Thorlabs Inc.). A PDMS reservoir with a diameter of 5 mm attached on top of the rubbery semiconducting nanofilm allowed the PBS solution to contact the nanofilm to build the optoelectronic interface. A custom-made two-terminal LabView coding equipped with PXL6363 was developed to acquire the transient photovoltages. Data were analyzed in MATLAB (MathWorks) and presented in OriginLab.

Stretchability test of RBOES

To evaluate stretchability, a thin PDMS sheet was used as a substrate. The Au nanomesh conductor was first attached to the PDMS with the Au layer facing up. Afterward, the rubbery semiconducting nanofilm was picked up from the water and placed on top of the Au nanomesh. Next, the PDMS sheet was mounted and fixed onto a custom-made tensile stretcher. To ensure proper contact during stretching, a droplet of liquid metal (gallium-indium eutectic, Sigma-Aldrich) was placed on the Au nanomesh as the electrical contact. The photovoltage of the RBOES was extracted under stretching with the aforementioned method.

HiPSC expansion and cardiac differentiation

The hiPSCs (SCVI20) used in this study were donated by the Stanford University Cardiovascular Institute Biobank. Cells were cultured and maintained in a feeder-free system of human embryonic stem cell–qualified Matrigel (Corning) and TeSR1 E8 (STEMCELL Technologies Inc., Cambridge, MA, USA) under standard culture conditions (37°C at 5% CO_2). Briefly, 1×10^5 cells were plated in TeSR E8 media supplemented with Y-27632 (10 μM, STEMCELL Technologies Inc., Vancouver, Canada). The medium was changed daily, and the cells were passaged using the cell dissociation recombinant enzymatic solution TrypLE Express (Gibco, Waltham, MA, USA). The CMs generated in this study were obtained by differentiating the hiPSCs using the STEMdiff Cardiomyocyte Differentiation Kit (STEMCELL Technologies Inc., Vancouver, Canada) as previously described (*46*). After the end of the differentiation protocol (day 15), the cells were harvested using the STEMdiff Cardiomyocyte Dissociation Kit (STEMCELL Technologies). The cells were washed two times with PBS, and 1-ml cardiomyocyte dissociation medium (37°C) was added per well. Culture plates were incubated for 15 min at 37°C and 5% CO_2. Afterward, the cells were dislodged by adding cardiomyocyte support medium and pipetting up and down 5 to 10 times. The cells were centrifugated at 300*g* for 5 min, the pellet was resuspended, and ~0.8×10^6 CMs were used for the stimulation.

Viability and staining assays

Using 1 ml of Accutase, the hiPSC-CMs were divided into single cells for 10 to 15 min. FlowBuffer-1 (Dulbecco's PBS with 0.5% bovine serum albumin) was used to resuspend the hiPSC-CMs after which they were stained using the appropriate conjugated primary antibodies. A BD Accuri C6 Plus flow cytometer was used to acquire the data, and the FlowJo software was used to process it. For immunophenotyping by immunofluorescence, differentiated CMs attached to the RBOES were fixed with 4% paraformaldehyde and stained with DAPI.

Immunophenotype characterization

Flow cytometry was performed to immunophenotype the cells before and after 5 days of culture with RBOES. The cells were fixed and permeabilized using the BD Cytofix/Cytoperm kit (BD Biosciences, San Diego, CA, USA), as previously reported (*46*). Briefly, cells were resuspended and incubated in 250 μl of BD Cytofix/Cytoperm solution for 20 min at 4°C and then centrifuged at 600*g* for 5 min. The cells were resuspended in BD Perm/Wash buffer and stained with Alexa Fluor 647 mouse anti-cTNT (BD Biosciences, catalog no. 565744) for 30 min at room temperature. The isotype Alexa Fluor 647 mouse IgG1 (BD Biosciences, catalog no. 557714) was used as a negative control. The gating strategy used to define $cTNT^+$ cells is demonstrated in fig. S16A.

Stimulation of the hiPSC-CMs

To maintain the RBOES on the bottom of the culture plates, the devices were mounted on a PDMS reservoir with a 5-mm-diameter opening. The PDMS reservoirs were well-sterilized before the attachment of the RBOES. PDMS reservoirs were pretreated for 24 hours with 1% penicillin-streptomycin (10 000 U ml^{-1}; Gibco, Grand Island, NY, USA) in PBS. Afterward, the PDMS reservoirs were washed three times with PBS solution. The PDMS reservoirs were placed in the center of the MEA plates (60EcoMEA-Glass, Multichannel Systems MCS GmbH, Reutlingen, German) pretreated with fibronectin (1 mg/ml, Sigma-Aldrich). The CMs were then seeded in the PDMS reservoir in the presence of the RBOES. Those MEA plates with CMs in the absence of the RBOES served as the control group. Last, CMs were incubated, and the medium was changed daily until experimentation.

CMs cultured for 4 or 5 days were used to validate the RBOES. The ECG signals of the CMs were monitored by the multichannel system (MEA2100 Lite, MultiChannel Systems MCS GmbH, Reutlingen, German). A green LED light (530 nm, M530L4-C5, Thorlabs Inc.) was passed through an amplifying lens to focus on the small spot atop the RBOES to stimulate the CMs to beat at the targeted beating rate. The light and recording equipment were kept in an incubator to maintain the temperature and pH level throughout the whole experiment. Before stimulation, the CMs were allowed to stabilize for 10 min; afterward, their ECG signals were recorded, and the spontaneous initial beating rate was determined. The targeted beating rates were chosen to be slightly higher than the spontaneous beating rate. A 4-min break was added after every 10-min light stimulation to avoid any long-term light toxicity (*12*). The ECG signals were recorded before stimulation (1 min), during stimulation (10 min), and after stimulation (1 min). This cyclic light stimulation ensures the successful stimulation of the CM beating without introducing any side effects.

Cadaver tissue preparation and potential recording

Yorkshire pig hearts (~ 6-month-old pig, 25 to 50 kg in weight) were used after euthanasia. A median sternotomy was performed to dissect and harvest the hearts and a sample of the intercostal nerve. After harvesting, the heart and nerve were perfused, rinsed, and washed with 1X PBS neutral buffer (Life Technologies, Carlsbad, CA). A portion of the left atrium and anterior epicardial left ventricle as well as the thoracic intercostal nerve were extracted and placed at the examination table. The rubbery semiconducting nanofilm side of the RBOES was directly placed in contact with the tissue surfaces. A green LED light (M530L4-C5, Thorlabs Inc.) with different frequencies was passed through an amplifying lens to focus at the top of the device. To measure the potential induced by the RBOES, two alligator/needle electrodes were connected to an interface board (RHD2000, Intan Technologies) via an amplifier board (RHD2216, Intan Technologies) with bipolar input channels. During measurement, the tissue surfaces were kept wet using a PBS solution. During the whole experiment, the temperature and moisture of the tissue were stably maintained.

Preparation of Langendorff-perfused rat hearts

Male CDF rats (200 to 300 g, Charles River Laboratories) were heparinized (1000 IU/kg i.p.) and anesthetized with isoflurane using an anesthesia induction chamber. After anesthesia induction, rats were transferred to the surgical table, where anesthesia was kept with a nose mask. A median sternotomy was performed to access the thoracic cavity, followed by opening the pericardial sac and heart excision. Excised hearts were placed in an ice-cold PBS buffer, and the aorta was cannulated using an 18-gauge cannula. Cannulated hearts were assembled in the Langendorff perfusion system (Radnoti) and perfused with warm (37°C) oxygenated Krebs-Henseleit buffer (118 mM NaCl, 4.7 mM KCl, 1.2 mM $MgSO_4$, 1.25 mM $CaCl_2$, 1.2 mM KH_2PO_4, 25 mM $NaHCO_3$, and 11 mM glucose). The solution was balanced by bubbling 95% O_2/5% CO_2 to a pH of 7.4. The aortic perfusion pressure was kept at 60 mmHg by a vented liquid column. Part of the perfusion system was assembled inside a cell culture incubator (Sanyo MCO19AIC) to maintain the physiological condition.

The myocardium was exposed by removing the epicardium using a scalpel to allow for direct interaction of the RBOES with the CMs.

Stimulation of perfused rat hearts

The green LED light (M530L4-C5, Thorlabs Inc.) was passed through an amplifying lens to focus on the small spot atop of the device to stimulate the rat heart to beat at the targeted beating rate. The light source was kept in the cell culture incubator (see preparation of the perfused rat heart) throughout the whole experiment. The LED light was modulated at the specific waveform pattern with a 100-ms duration by a function generator. The ECG signals were recorded through sutured electrodes at the apex (working electrode) and left (ground electrode) atrial appendage and the back side of the right atrium (reference electrode). Before stimulation, the ECG morphology, frequency, and stability were monitored for 10 min by a LabChart 8 software coupled with PowerLab 8/35 and animal BioAmp (AD instruments; fig. S25C) after the start of the Langendorff perfusion to evaluate the heart recovery. The spontaneous beating rate was determined, and the targeted beating rate was set to be slightly higher than the spontaneous beating rate. The light was continuously applied to stimulate the heart until the targeted beating rate was achieved. Meanwhile, the temperature mapping of the RBOES during long-term optical stimulation was obtained by an infrared camera (FLIR ONE Pro, FLIR Systems).

Supplementary Materials

The PDF file includes:

Figs. S1 to S28
Legend for movie S1

Other Supplementary Material for this manuscript includes the following:

Movie S1

REFERENCES AND NOTES

1. J. F. Zimmerman, B. Tian, Nongenetic optical methods for measuring and modulating neuronal response. *ACS Nano* **12**, 4086–4095 (2018).
2. R. Parameswaran, J. L. Carvalho-de-Souza, Y. Jiang, M. J. Burke, J. F. Zimmerman, K. Koehler, A. W. Phillips, J. Yi, E. J. Adams, F. Bezanilla, B. Tian, Photoelectrochemical modulation of neuronal activity with free-standing coaxial silicon nanowires. *Nat. Nanotechnol.* **13**, 260–266 (2018).
3. K. Mathieson, J. Loudin, G. Goetz, P. Huie, L. Wang, T. I. Kamins, L. Galambos, R. Smith, J. S. Harris, A. Sher, D. Palanker, Photovoltaic retinal prosthesis with high pixel density. *Nat. Photonics* **6**, 391–397 (2012).
4. P.-H. Prévot, K. Gehere, F. Arcizet, H. Akolkar, M. A. Khoei, K. Blaize, O. Oubari, P. Daye, M. Lanoë, M. Valet, S. Dalouz, P. Langlois, E. Esposito, V. Forster, E. Dubus, N. Wattiez, E. Brazhnikova, C. Nouvel-Jaillard, Y. LeMer, J. Demilly, C.-M. Fovet, P. Hantraye, M. Weissenburger, H. Lorach, E. Bouillet, M. Deterre, R. Hornig, G. Buc, J.-A. Sahel, G. Chenegros, P. Pouget, R. Benosman, S. Picaud, Behavioural responses to a photovoltaic subretinal prosthesis implanted in non-human primates. *Nat. Biomed. Eng.* **4**, 172–180 (2020).
5. D. Palanker, Y. Le Mer, S. Mohand-Said, J. A. Sahel, Simultaneous perception of prosthetic and natural vision in AMD patients. *Nat. Commun.* **13**, 513 (2022).
6. S. M. Won, E. Song, J. T. Reeder, J. A. Rogers, Emerging modalities and implantable technologies for neuromodulation. *Cell* **181**, 115–135 (2020).
7. S. M. Won, L. Cai, P. Gutruf, J. A. Rogers, Wireless and battery-free technologies for neuroengineering. *Nat. Biomed. Eng.* **7**, 405–423 (2023).
8. Y. Lu, Y. Jia, C. Yu, Recent advances in power supply strategies for untethered neural implants. *J. Micromech. Microeng.* **31**, 104003 (2021).
9. R. Feiner, T. Dvir, Tissue–Electronics interfaces: From implantable devices to engineered tissues. *Nat. Rev. Mater.* **3**, 17076 (2018).
10. G. Gagnon-Turcotte, Y. LeChasseur, C. Bories, Y. Messaddeq, Y. De Koninck, B. Gosselin, A wireless headstage for combined optogenetics and multichannel electrophysiological recording. *IEEE Trans. Biomed. Circuits Syst.* **11**, 1–14 (2017).
11. G. Yao, L. Kang, J. Li, Y. Long, H. Wei, C. A. Ferreira, J. J. Jeffery, Y. Lin, W. Cai, X. Wang, Effective weight control via an implanted self-powered vagus nerve stimulation device. *Nat. Commun.* **9**, 5349 (2018).
12. R. Parameswaran, K. Koehler, M. Y. Rotenberg, M. J. Burke, J. Kim, K.-Y. Jeong, B. Hissa, M. D. Paul, K. Moreno, N. Sarma, T. Hayes, E. Sudzilovsky, H.-G. Park, B. Tian, Optical stimulation of cardiac cells with a polymer-supported silicon nanowire matrix. *Proc. Natl. Acad. Sci. U.S.A.* **116**, 413–421 (2019).
13. M. Silverå Ejneby, M. Jakešová, J. J. Ferrero, L. Migliaccio, I. Sahalianov, Z. Zhao, M. Berggren, D. Khodagholy, V. Đerek, J. N. Gelinas, E. D. Głowacki, Chronic electrical stimulation of peripheral nerves via deep-red light transduced by an implanted organic photocapacitor. *Nat. Biomed. Eng.* **6**, 741–753 (2022).
14. Z. Liu, B. Wen, L. Cao, S. Zhang, Y. Lei, G. Zhao, L. Chen, J. Wang, Y. Shi, J. Xu, X. Pan, L. Yu, Photoelectric cardiac pacing by flexible and degradable amorphous Si radial junction stimulators. *Adv. Healthc. Mater.* **9**, e1901342 (2020).
15. J. Tang, N. Qin, Y. Chong, Y. Diao, Yiliguma, Z. Wang, T. Xue, M. Jiang, J. Zhang, G. Zheng, Nanowire arrays restore vision in blind mice. *Nat. Commun.* **9**, 786 (2018).
16. X. Lin, Y. Liu, A. Bai, H. Cai, Y. Bai, W. Jiang, H. Yang, X. Wang, L. Yang, N. Sun, H. Gao, A viscoelastic adhesive epicardial patch for treating myocardial infarction. *Nat. Biomed. Eng.* **3**, 632–643 (2019).
17. J. Park, S. Choi, A. H. Janardhan, S.-Y. Lee, S. Raut, J. Soares, K. Shin, S. Yang, C. Lee, K.-W. Kang, H. R. Cho, S. J. Kim, P. Seo, W. Hyun, S. Jung, H.-J. Lee, N. Lee, S. H. Choi, M. Sacks, N. Lu, M. E. Josephson, T. Hyeon, D.-H. Kim, H. J. Hwang, Electromechanical cardioplasty using a wrapped elasto-conductive epicardial mesh. *Sci. Transl. Med.* **8**, 344ra386 (2016).
18. L. Xu, S. R. Gutbrod, A. P. Bonifas, Y. Su, M. S. Sulkin, N. Lu, H.-J. Chung, K.-I. Jang, Z. Liu, M. Ying, C. Lu, R. C. Webb, J.-S. Kim, J. I. Laughner, H. Cheng, Y. Liu, A. Ameen, J.-W. Jeong, G.-T. Kim, Y. Huang, I. R. Efimov, J. A. Rogers, 3D multifunctional integumentary membranes for spatiotemporal cardiac measurements and stimulation across the entire epicardium. *Nat. Commun.* **5**, 3329 (2014).
19. Y. Jiang, X. Li, B. Liu, J. Yi, Y. Fang, F. Shi, X. Gao, E. Sudzilovsky, R. Parameswaran, K. Koehler, V. Nair, J. Yue, K. Guo, Y. Fang, H.-M. Tsai, G. Freyermuth, R. C. S. Wong, C.-M. Kao, C.-T. Chen, A. W. Nicholls, X. Wu, G. M. G. Shepherd, B. Tian, Rational design of silicon structures for optically controlled multiscale biointerfaces. *Nat. Biomed. Eng.* **2**, 508–521 (2018).
20. N. Martino, P. Feyen, M. Porro, C. Bossio, E. Zucchetti, D. Ghezzi, F. Benfenati, G. Lanzani, M. R. Antognazza, Photothermal cellular stimulation in functional bio-polymer interfaces. *Sci. Rep.* **5**, 8911 (2015).
21. M. Tallawi, R. Rai, A. R. Boccaccini, K. E. Aifantis, Effect of substrate mechanics on cardiomyocyte maturation and growth. *Tissue Eng. Part B Rev.* **21**, 157–165 (2014).
22. D. McCoul, W. Hu, M. Gao, V. Mehta, Q. Pei, Recent advances in stretchable and transparent electronic materials. *Adv. Electron. Mater.* **2**, 1500407 (2016).
23. Y. Wang, S. Lee, H. Wang, Z. Jiang, Y. Jimbo, C. Wang, B. Wang, J. Kim Jae, M. Koizumi, T. Yokota, T. Someya, Robust, self-adhesive, reinforced polymeric nanofilms enabling gas-permeable dry electrodes for long-term application. *Proc. Natl. Acad. Sci. U.S.A.* **118**, e2111904118 (2021).
24. S. Lee, D. Sasaki, D. Kim, M. Mori, T. Yokota, H. Lee, S. Park, K. Fukuda, M. Sekino, K. Matsuura, T. Shimizu, T. Someya, Ultrasoft electronics to monitor dynamically pulsing cardiomyocytes. *Nat. Nanotechnol.* **14**, 156–160 (2019).
25. M. Kaltenbrunner, T. Sekitani, J. Reeder, T. Yokota, K. Kuribara, T. Tokuhara, M. Drack, R. Schwödiauer, I. Graz, S. Bauer-Gogonea, S. Bauer, T. Someya, An ultra-lightweight design for imperceptible plastic electronics. *Nature* **499**, 458–463 (2013).
26. R. A. Nawrocki, H. Jin, S. Lee, T. Yokota, M. Sekino, T. Someya, Self-adhesive and ultra-conformable, sub-300 nm dry thin-film electrodes for surface monitoring of biopotentials. *Adv. Funct. Mater.* **28**, 1803279 (2018).
27. W.-H. Yeo, Y.-S. Kim, J. Lee, A. Ameen, L. Shi, M. Li, S. Wang, R. Ma, S. H. Jin, Z. Kang, Y. Huang, J. A. Rogers, Multifunctional epidermal electronics printed directly onto the skin. *Adv. Mater.* **25**, 2773–2778 (2013).
28. E. Mosconi, P. Salvatori, M. I. Saba, A. Mattoni, S. Bellani, F. Bruni, B. Santiago Gonzalez, M. R. Antognazza, S. Brovelli, G. Lanzani, H. Li, J.-L. Brédas, F. De Angelis, Surface polarization drives photoinduced charge separation at the P3HT/water interface. *ACS Energy lett.* **1**, 454–463 (2016).
29. T. Flores, G. Goetz, X. Lei, D. Palanker, Optimization of return electrodes in neurostimulating arrays. *J. Neural Eng.* **13**, 036010 (2016).
30. Z. Peng, K. Xian, Y. Cui, Q. Qi, J. Liu, Y. Xu, Y. Chai, C. Yang, J. Hou, Y. Geng, L. Ye, Thermoplastic elastomer tunes phase structure and promotes stretchability of high-efficiency organic solar cells. *Adv. Mater.* **33**, e2106732 (2021).
31. L. Ferlauto, M. J. I. Airaghi Leccardi, N. A. L. Chenais, S. C. A. Gilliéron, P. Vagni, M. Bevilacqua, T. J. Wolfensberger, K. Sivula, D. Ghezzi, Design and validation of a foldable and photovoltaic wide-field epiretinal prosthesis. *Nat. Commun.* **9**, 992 (2018).
32. S. Lee, A. Reuveny, J. Reeder, S. Lee, H. Jin, Q. Liu, T. Yokota, T. Sekitani, T. Isoyama, Y. Abe, Z. Suo, T. Someya, A transparent bending-insensitive pressure sensor. *Nat. Nanotechnol.* **11**, 472–478 (2016).
33. H. Wu, D. Kong, Z. Ruan, P.-C. Hsu, S. Wang, Z. Yu, T. J. Carney, L. Hu, S. Fan, Y. Cui, A transparent electrode based on a metal nanotrough network. *Nat. Nanotechnol.* **8**, 421–425 (2013).

34. F. Wei, M. Pourrier, D. G. Strauss, N. Stockbridge, L. Pang, Effects of electrical stimulation on hiPSC-CM responses to classic ion channel blockers. *Toxicol. Sci.* **174**, 254–265 (2020).
35. S.-H. Sunwoo, M.-J. Cha, S. I. Han, H. Kang, Y. S. Cho, D.-H. Yeom, C. S. Park, N. K. Park, S. W. Choi, S. J. Kim, G. D. Cha, D. Jung, S. Choi, S. Oh, G.-B. Nam, T. Hyeon, D.-H. Kim, S.-P. Lee, Ventricular tachyarrhythmia treatment and prevention by subthreshold stimulation with stretchable epicardial multichannel electrode array. *Sci. Adv.* **9**, eadf6856 (2023).
36. T. Noboru, S. Kiro, The influence of sympathetic stimulation on transmembrane potentials in the SA node. *J. Pharmacol. Exp. Ther.* **159**, 298 (1968).
37. Y. Fang, A. Prominski, M. Y. Rotenberg, L. Meng, H. Acarón Ledesma, Y. Lv, J. Yue, E. Schaumann, J. Jeong, N. Yamamoto, Y. Jiang, B. Elbaz, W. Wei, B. Tian, Micelle-enabled self-assembly of porous and monolithic carbon membranes for bioelectronic interfaces. *Nat. Nanotechnol.* **16**, 206–213 (2021).
38. K. Sim, F. Ershad, Y. Zhang, P. Yang, H. Shim, Z. Rao, Y. Lu, A. Thukral, A. Elgalad, Y. Xi, B. Tian, D. A. Taylor, C. Yu, An epicardial bioelectronic patch made from soft rubbery materials and capable of spatiotemporal mapping of electrophysiological activity. *Nat. Electron.* **3**, 775–784 (2020).
39. J. Liu, X. Zhang, Y. Liu, M. Rodrigo, P. D. Loftus, J. Aparicio-Valenzuela, J. Zheng, T. Pong, K. J. Cyr, M. Babakhanian, J. Hasi, J. Li, Y. Jiang, C. J. Kenney, P. J. Wang, A. M. Lee, Z. Bao, Intrinsically stretchable electrode array enabled in vivo electrophysiological mapping of atrial fibrillation at cellular resolution. *Proc. Natl. Acad. Sci. U.S.A.* **117**, 14769–14778 (2020).
40. S. I. Park, D. S. Brenner, G. Shin, C. D. Morgan, B. A. Copits, H. U. Chung, M. Y. Pullen, K. N. Noh, S. Davidson, S. J. Oh, J. Yoon, K.-I. Jang, V. K. Samineni, M. Norman, J. G. Grajales-Reyes, S. K. Vogt, S. S. Sundaram, K. M. Wilson, J. S. Ha, R. Xu, T. Pan, T. Kim, Y. Huang, M. C. Montana, J. P. Golden, M. R. Bruchas, R. W. Gereau, J. A. Rogers, Soft, stretchable, fully implantable miniaturized optoelectronic systems for wireless optogenetics. *Nat. Biotechnol.* **33**, 1280–1286 (2015).
41. P. Gutruf, R. T. Yin, K. B. Lee, J. Ausra, J. A. Brennan, Y. Qiao, Z. Xie, R. Peralta, O. Talarico, A. Murillo, S. W. Chen, J. P. Leshock, C. R. Haney, E. A. Waters, C. Zhang, H. Luan, Y. Huang, G. Trachiotis, I. R. Efimov, J. A. Rogers, Wireless, battery-free, fully implantable multimodal and multisite pacemakers for applications in small animal models. *Nat. Commun.* **10**, 5742 (2019).
42. P. M. Boyle, J. C. Williams, C. M. Ambrosi, E. Entcheva, N. A. Trayanova, A comprehensive multiscale framework for simulating optogenetics in the heart. *Nat. Commun.* **4**, 2370 (2013).
43. J. Yu, K. Chen, R. V. Lucero, C. M. Ambrosi, E. Entcheva, Cardiac optogenetics: Enhancement by all-trans-retinal. *Sci. Rep.* **5**, 16542 (2015).
44. A. Miyamoto, S. Lee, N. F. Cooray, S. Lee, M. Mori, N. Matsuhisa, H. Jin, L. Yoda, T. Yokota, A. Itoh, M. Sekino, H. Kawasaki, T. Ebihara, M. Amagai, T. Someya, Inflammation-free, gas-permeable, lightweight, stretchable on-skin electronics with nanomeshes. *Nat. Nanotechnol.* **12**, 907–913 (2017).
45. S. Lee, S. Franklin, F. A. Hassani, T. Yokota, M. O. G. Nayeem, Y. Wang, R. Leib, G. Cheng, D. W. Franklin, T. Someya, Nanomesh pressure sensor for monitoring finger manipulation without sensory interference. *Science* **370**, 966–970 (2020).
46. F. C. P. Mesquita, J. Morrissey, P.-F. Lee, G. Monnerat, Y. Xi, H. Andersson, F. C. S. Nogueira, G. B. Domont, L. C. Sampaio, C. Hochman-Mendez, D. A. Taylor, Cues from human atrial extracellular matrix enrich the atrial differentiation of human induced pluripotent stem cell-derived cardiomyocytes. *Biomater. Sci.* **9**, 3737–3749 (2021).

Acknowledgments: We would like to thank the Texas Heart Institute Cardiovascular Research Laboratories for their contribution to the porcine tissue sharing resource and Gil Costas DMV for the animal care and welfare. **Funding:** C.Y. would like to acknowledge the funding support by National Science Foundation (CBET-2227063, CNS-2227062, and EFRI-1935291), the National Institute of Health (R21EB026175 and 1R21EB030257-01), and the Office of Naval Research (N00014-18-1-2338). **Author contributions:** Z.R. and C.Y. conceived the concept. Z.R. and C.Y. initiated and led the whole project. Z.R., Y.-S.G., B.K., and Y.L. prepared the materials and fabricated the devices. Z.R., S.P., H.S., K.C., and W.W. contributed to the material characterization. F.E. assisted in the design and data collection of the biological experiments. F.C.P.M., E.C.d.C., M.A.M-.G., A.M.-R., T.H., Z.R., F.E., A.E., and C.H.-M. performed the in vitro and animal experiments. Z.R., F.E., E.C., and C.Y. analyzed the experimental data. Z.R., F.M., E.C.d.C., M.A.M-.G., and C.Y. prepared the manuscript. Z.R., F.E., and C.Y. revised the manuscript. All authors reviewed and approved the manuscript. **Competing interests:** Z.R., F.E., and C.Y. have submitted an invention disclosure based on the research described in this manuscript. The other authors declare that they have no competing interests. **Data and materials availability:** All data needed to evaluate the conclusions in the paper are present in the paper and/or the Supplementary Materials.

Submitted 4 July 2024
Accepted 30 October 2024
Published 6 December 2024
10.1126/sciadv.adq5061